Developmental Cell, Volume *22*

Supplemental Information

Secreted VAPB/ALS8 Major Sperm Protein Domains Modulate Mitochondrial Localization and Morphology via Growth Cone Guidance Receptors

Sung Min Han, Hiroshi Tsuda, Youfeng Yang, Jack Vibbert, Pauline Cottee, Se-Jin Lee, Jessica Winek, Claire Haueter, Hugo J. Bellen, and Michael A. Miller

Supplemental Inventory

Figure S1, related to Figure 1; *C. elegans* muscle mitochondria in wild-type and mutant backgrounds.

Figure S2, related to Figures 2 and 3; VPR-1 expression pattern in adult worms.

Figure S3, related to Figure 4; MSP domain binding to cell surface receptors.

Figure S4, related to Figure 5; Oocyte mitochondrial morphology in the presence and absence of secreted MSP domains provided by sperm.

Figure S5, related to Figure 8; RNAi of specific actin regulators causes muscle mitochondrial morphology defects.

Table S1, related to Figures 1, 3, 6, 7, and 8; Quantification of muscle mitochondrial localization and morphology.

Table S2, related to Figure 5; RNAi screen for MSP receptors affecting mitochondria.

Movies S1-S4, related to Figure 3; Time-lapse videos of muscle mitochondrial dynamics.

Supplemental Data

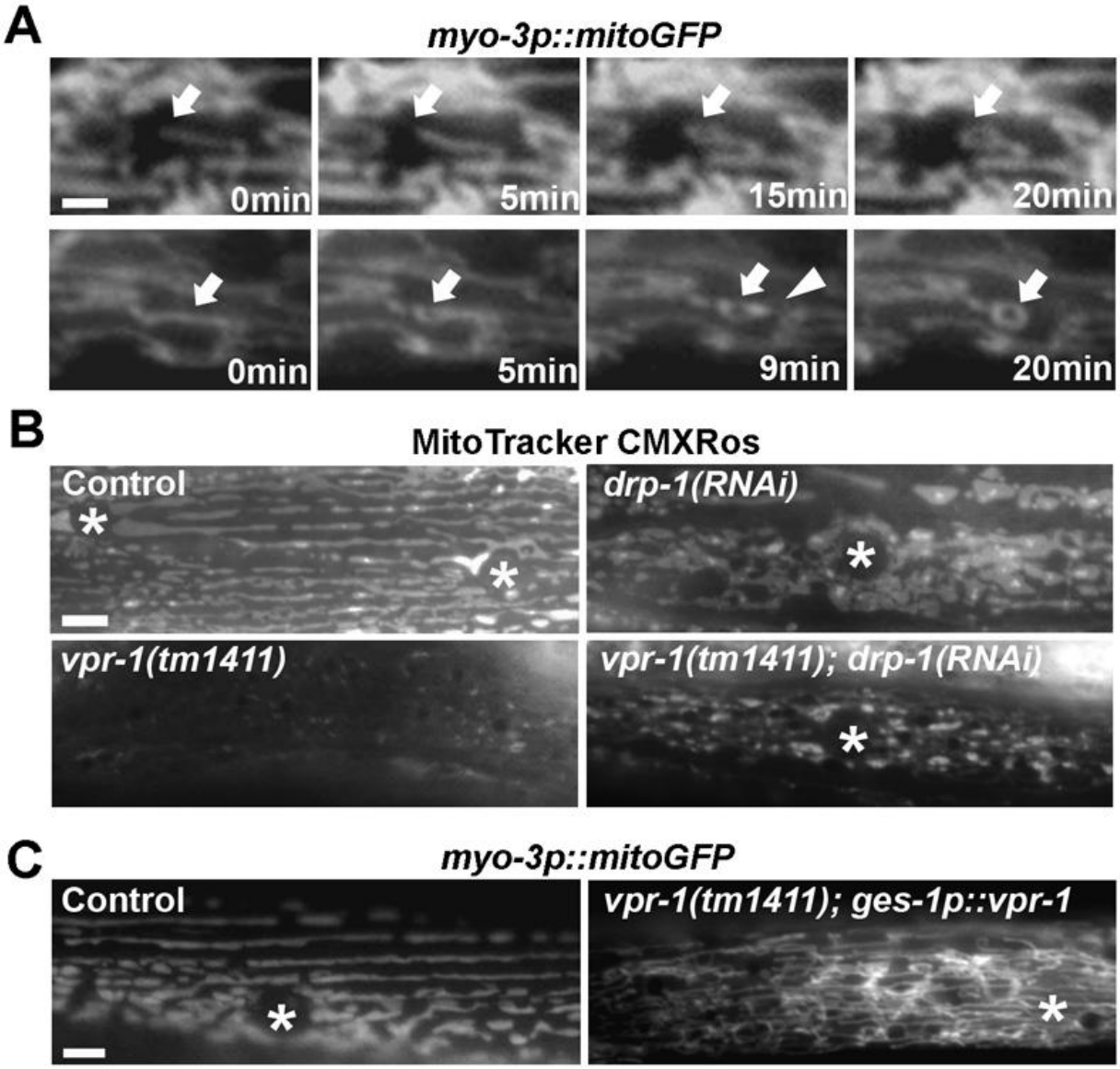

Figure S1. Mitochondria in *vpr-1* mutant body wall muscle
(A) *vpr-1(tm1411)* mutant image sequences showing formation of ring-shaped mitochondria (arrows). In the top sequence, a branch forms a ring-shaped structure (arrow), likely by fusion of the branch tip with the midbody or by abnormal fission within the branch tip. In the bottom sequence, a ring-shaped structure (arrow) forms in the middle of a branch and then one end of the branch detaches from the network (arrowhead). Bar, 2 µm
(B) MitoTracker CMXRos staining of wild-type and mutant muscle. Asterisks indicate nucleus. Bar, 5 µm
(C) Muscle mitochondrial networks in control and *vpr-1(tm1411)* mutants expressing *vpr-1* in the intestine using the *ges-1* promoter. Asterisks indicate nucleus. Bar, 5 µm.

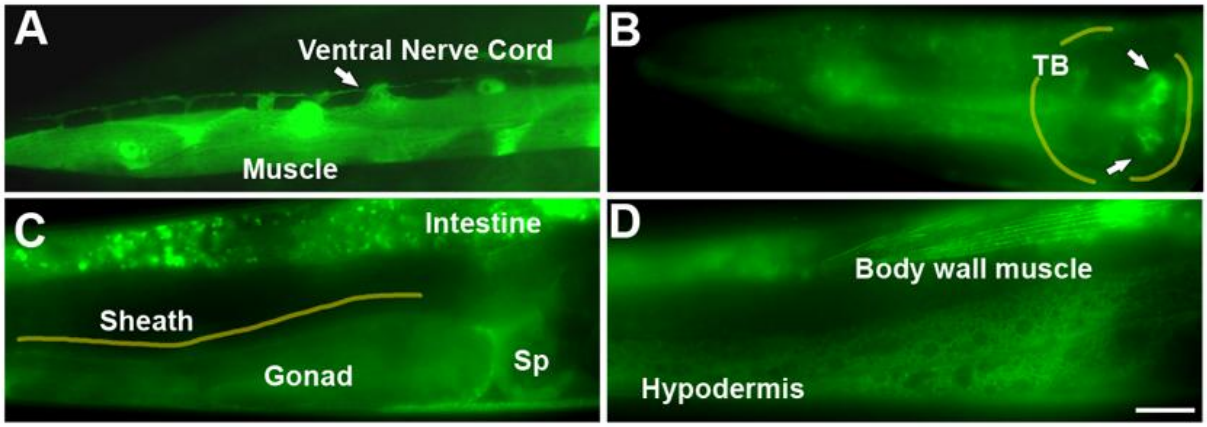

Figure S2. *vpr-1* expression pattern in adult hermaphrodites

(A) Transgenic strain expressing GFP under control of ~2.2 kb DNA upstream of the *vpr-1* gene. Transgenics show broad and sometimes mosaic patterns of GFP expression in the intestine, gonad, hypodermal cells, muscles, and the nervous system.

(B-D) Transgenic strains expressing VPR-1::GFP under control of ~2.2 kb DNA upstream of the *vpr-1* gene. VPR-1::GFP expression is seen in head neurons (B, arrows) near the terminal bulb (TB), gonadal sheath cells (C), hypodermal cells, and body wall muscle cells (D). Bar, 10 μm.

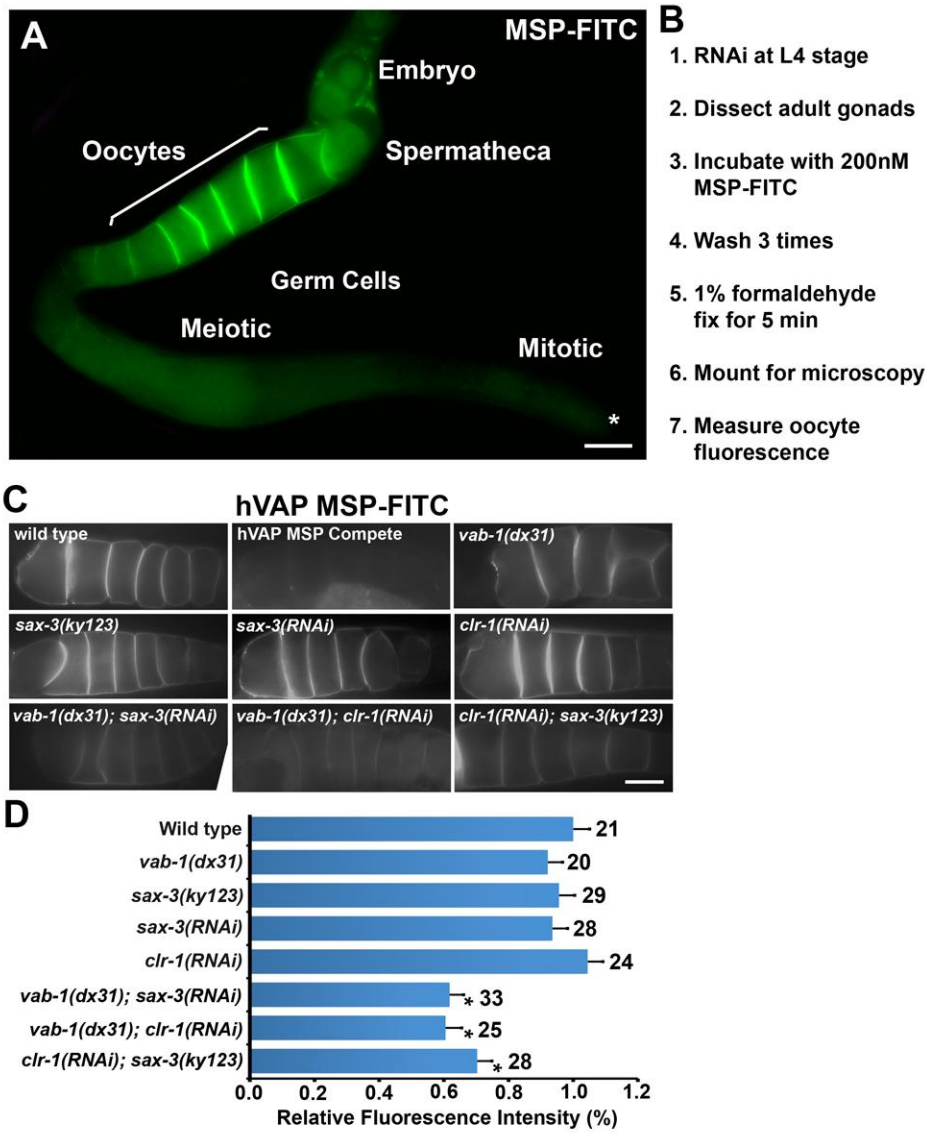

Figure S3. MSP-FITC and hVAP MSP-FITC binding to *C. elegans* oocytes

(A) MSP and vMSP-FITC bind to multiple receptors expressed specifically in oocytes (Miller et al., 2003; Tsuda et al., 2008). See Fig. 5A for diagram of the gonad. Asterisk indicates distal tip cell. Bar, 20 µm.

(B) Procedure for identifying MSP domain receptors. Receptor candidates were selected for screening based on published microarray and *in situ* hybridization data (Table S2).

(C) Representative images of human VAPB (hVAP) MSP-FITC binding to wild-type and mutant gonads. Compete represents pre-incubation with a 20-fold molar excess of unlabelled hVAP MSP before the assay. Unlike MSP-FITC, we did not detect significant reductions in hVAP MSP-FITC to oocytes lacking any single receptor candidate, even the known MSP receptor VAB-1 EphR. Loss of multiple receptors causes a synergistic loss of hVAP MSP-FITC binding. Similar results were observed with the VPR-1 MSP domain. Thus, VAP MSP domains may bind to multiple receptors with compensatory binding mechanisms. Bar, 20 µm.

(D) Quantitative data for human hVAP MSP-FITC binding to oocytes. *$P < 0.001$ compared to wild type. Error bars represent SEM.

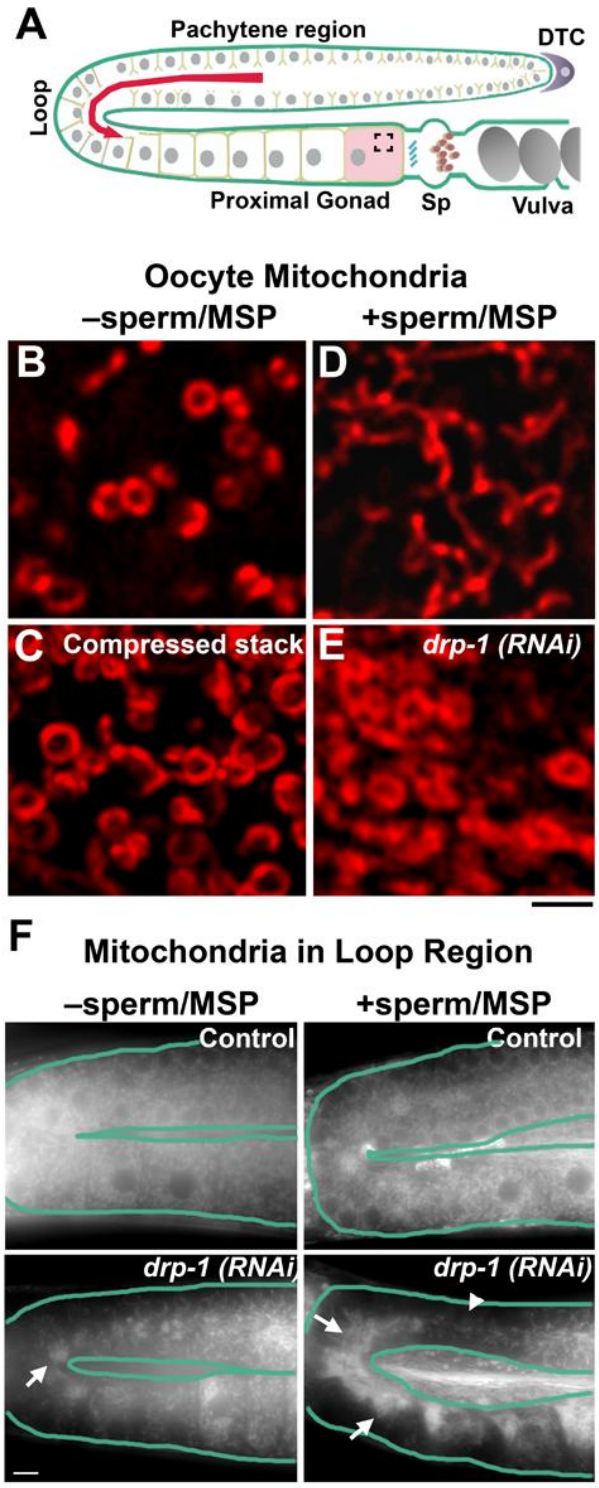

Figure S4. Oocyte mitochondria in the presence and absence of sperm/MSP

(A) Diagram of the *C. elegans* adult gonad. Sperm within the spermatheca (Sp) secrete MSPs that bind to multiple oocyte receptors (Han et al., 2010). Ring-shaped mitochondria were observed in oocytes within proximal gonads lacking sperm. Pink shade shows the oocyte closest to the spermatheca and brackets indicate region from which mitochondrial images were taken in

panels B-C. Arrow indicates direction of MSP-induced mitochondrial transport into growing oocytes. DTC, distal tip cell.

(B-E) Deconvolved confocal images of Rhodamine 6g-labelled oocyte mitochondria in the presence and absence of sperm/MSP. For confocal images, a stack with 200 nm spacing was taken in hermaphrodites and unmated females. Panel C shows a compressed 3.0 µm stack. The mitochondrial aggregate shown in panel E was located in the loop region (see panel A). Bar, 2 µm.

(F) Rhodamine 6g-labelled mitochondria in control and *drp-1* RNAi hermaphrodite and unmated female gonads (spermless). We used RNAi conditions that diminish, but do not eliminate DRP-1 function, which is essential for germ line development. *drp-1* RNAi hermaphrodites (with sperm) contain large mitochondrial aggregates in oocytes (arrows), as previously reported (Labrousse et al., 1999). 3D confocal microscopy indicates that these aggregates often contain abundant ring-shaped mitochondria connected by long tubules (panel E). *drp-1* reduction of function causes much smaller mitochondrial aggregates in unmated females lacking sperm/MSP than in hermaphrodites and mated females containing sperm/MSP. Providing sperm to these *drp-1* RNAi unmated females induces mitochondrial aggregation in developing oocytes. Oocyte mitochondrial aggregates in *drp-1* RNAi gonads initially form in syncytial oocyte precursors. Arrowhead indicates loss of mitochondria from these precursors. Previous studies have shown that MSP induces a robust increase in the mitochondrial transport rate from oocyte precursors to growing oocytes (panel A, arrow in loop region) (Govindan et al., 2009; Wolke et al., 2007). These results suggest that DRP-1 activity is necessary for mitochondrial division prior to or during transport. Unmated female gonads are less dependent on *drp-1* because mitochondrial transport is slow, allowing for more time to divide. Thus, extracellular MSPs may influence DRP-1 function critical for mitochondrial shape-changes and transport.

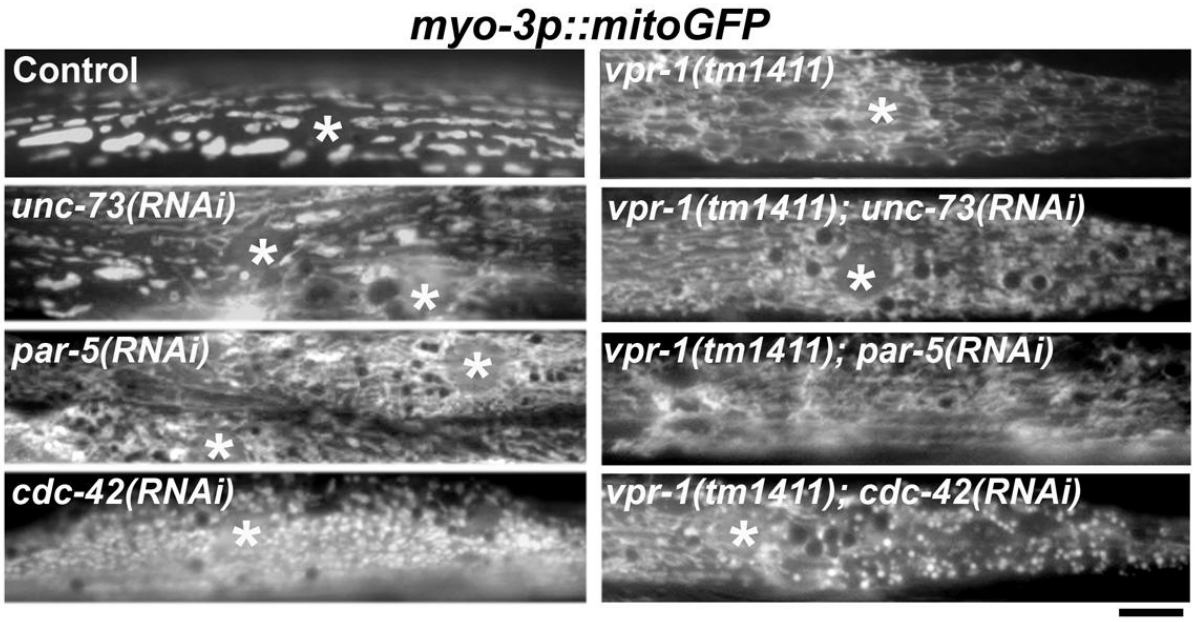

Figure S5. RNAi of genes encoding actin regulators affect muscle mitochondrial position and morphology

unc-73 Trio encodes a Rac and Rho guanine nucleotide exchange factor that directly interacts with the SAX-3 Robo intracellular domain (Steven et al., 1998; Watari-Goshima et al., 2007). Furthermore, mammalian Trio interacts with the LAR receptor intracellular domain (Debant et al., 1996). CDC-42 acts downstream of Robo and Lar receptors during growth cone guidance decisions (Bateman et al., 2000; Wong et al., 2001). PAR-5 encodes a 14-3-3 homolog that regulates actin remodeling downstream of numerous receptors. RNAi was initiated at the L1 stage to bypass most developmental requirements. To examine the signaling hierarchy, we tested the genetic relationship between each gene and *vpr-1*. *unc-73* RNAi in *vpr-1* null mutants results in identical mitochondrial defects as *vpr-1* null mutants. Similar results are observed with *par-5*. Thus, *vpr-1* may act in the same genetic pathway as *unc-73* and *par-5*. *cdc-42* RNAi in *vpr-1* null mutants results in a mixed phenotype. Some mitochondria resemble the globular mitochondria observed in *cdc-42* RNAi animals, whereas other mitochondria are elongated similar to *vpr-1* mutants. We interpret these data as evidence that *cdc-42* acts downstream of *vpr-1*, with the incomplete suppression due to inefficient RNAi or a parallel effector(s). These data suggest that Rho family GTPases mediate vMSP/Robo/Lar signaling to mitochondria. Defects were not observed in *ced-10, mig-10, par-6, wve-1,* and *gex-3* RNAi muscle. Asterisks indicate nucleus. Bar, 5 µm.

Table S1. Quantification of mitochondrial morphology and position in wild-type and mutant body wall muscle. Data quantified from transgenic strains expressing mitoGFP, except where indicated.

Genotype	Tubule length (μm±SD)	Tubule branch points/mm	Tubule cross-sectional area (μm^2±SD)[a]	Tubules aligned with I-bands (%)	Muscles quantified
1. Wild type	7.52±3.86 N = 100	20.3	0.327±0.24 N = 36	84.7 N = 98	10
2. *vpr-1(tm1411)*	24.04±7.28[b] N = 14	380.27	0.099±0.05 N = 79	33.1 N = 680	9
3. *sax-3(ky123)*[c]	28.59±6.93[b] N = 13	295.86	0.084±0.06 N = 30	38.8 N = 803	6
4. *clr-1* (RNAi)	1.89±0.65 N = 65	0	ND	78.8 N = 307	5
5. *vpr-1(tm1411); sax-3(ky123)*	ND	ND	0.097±0.05 N = 53	ND	NA
6. *vpr-1(tm1411); clr-1* (RNAi)	5.86±3.88 N = 125	9.82	ND	83.2 N = 119	6
7. *arx-2* (RNAi); *vpr-1(tm1411)*	5.33±3.85 N = 121	5.82	ND	90.6 N = 181	8
8. *arx-2* (RNAi)	3.21±1.24 N = 89	0	ND	95.6 N = 136	5

[a] Quantified from transmission electron micrographs (N = no. of mitochondria).
[b] Quantified by taking the shortest distance between two free tubule ends.
[c] *sax-3(ky123)* phenotypes are 63.6% penetrant. Data taken from abnormal muscle with the exception of cross sectional area measurements.
ND, not determined.
NA, not applicable.

Table S2. RNAi screen summary. The 40 potential receptors were identified from DNA microarray data comparing adult hermaphrodites undergoing oogenesis to those undergoing spermatogenesis (Reinke et al., 2004). The top 3000 genes were searched for those encoding known receptors or those with predicted transmembrane domains that might span the plasma membrane. MSP and VAP MSP domains bind to oocyte plasma membranes, but not sperm plasma membranes (Miller et al., 2003; Tsuda et al., 2008). For MSP-FITC binding, feeding RNAi was initiated at the L4 stage. For Rhodamine 6g mitochondrial screening, feeding RNAi was initiated following embryo hatching and mitochondria were scored in adults.

Gene	**Description**	**Oocyte MSP-FITC Binding**	**Body Wall Muscle Mito**	**Oocyte Mito**
vab-1	Eph protein-tyrosine kinase receptor homolog	Reduced	No effect	No effect
stl-1	Contains stomatin and putative transmembrane domains	No effect	No effect	No effect
clr-1	Lar-like receptor protein-tyrosine phosphatase	Reduced	Abnormal	Abnormal*
cab-1	Novel gene predicted to encode a transmembrane protein	No effect	No effect	No effect
tsp-12	Tetraspanin	No effect	No effect	No effect
rme-2	Low density lipoprotein receptor mediating yolk endocytosis	No effect	No effect	Abnormal**
egg-1	Receptor with low density lipoprotein repeats	No effect	No effect	No effect
sax-3	Robo receptor homolog	Reduced	Abnormal	Abnormal*
lat-1	Latrotoxin receptor homolog, G-protein coupled receptor	Reduced	No effect	Abnormal*
daf-2	Insulin/IGF receptor homolog	No effect	Abnormal	No effect
W08F4.3	Novel gene predicted to encode a transmembrane protein	No effect	No effect	No effect
egg-2	Receptor with low density lipoprotein repeats	No effect	No effect	No effect
unc-40	Netrin receptor homolog	No effect	No effect	No effect
K07A12.2	Leucine-rich repeat receptor protein	Reduced	No effect	No effect
C15C8.4	human alpha-2-macroglobuin receptor-associated protein-like	No effect	No effect	No effect
mom-5	Frizzled receptor homolog	No effect	No effect	No effect
cam-1/kin-8	ROR protein-tyrosine kinase receptor homolog	Reduced	No effect	No effect
C13B9.4	G-protein coupled receptor	No effect	No effect	No effect

ZK418.5	Novel gene predicted to encode a transmembrane protein	No effect	No effect	No effect
gex-3	Drosophila Dhem transmembrane protein-like	No effect	No effect	No effect
C36B7.6	Novel gene predicted to encode transmembrane protein	No effect	No effect	No effect
rom-1	Rhomboid-like transmembrane protein	No effect	No effect	No effect
C03A3.2	Transmembrane protein, may be transporter	No effect	No effect	No effect
sup-17	Kuzbanian metalloprotease homolog	No effect	Larval arrest	Larval arrest
odr-4	Transmembrane protein, may be type II	No effect	Abnormal	No effect
R166.2	Novel gene predicted to encode transmembrane protein	No effect	No effect	No effect
F26E4.11	Transmembrane protein related to autocrine motility factor receptor	No effect	No effect	No effect
C56C10.10	Similar to aryl-hydrocarbon receptor-interacting protein	No effect	No effect	No effect
cfz-2	Frizzled receptor homolog	No effect	No effect	No effect
srx-96	7-transmembrane serpentine receptor	No effect	Abnormal	No effect
srj-35	7-transmembrane serpentine receptor	No effect	No effect	No effect
sre-23	7-transmembrane serpentine receptor	No effect	No effect	No effect
srj-29	7-transmembrane serpentine receptor	No effect	No effect	No effect
D1054.1	Contain phospholipase and possible transmembrane domain	No effect	No effect	No effect
F14E5.2	Contains cysteine-rich and putative transmembrane domains	No effect	No effect	No effect
nra-3	Novel gene predicted to encode a transmembrane protein	No effect	No effect	No effect
F44F4.1	Novel gene predicted to encode a transmembrane protein	No effect	No effect	No effect
C53D6.4	Novel gene predicted to encode a transmembrane protein	No effect	No effect	No effect
R09F10.8	Novel gene predicted to encode a transmembrane protein	No effect	No effect	No effect
gnrr-2	G-protein coupled receptor	No effect	No effect	Abnormal*

*, Defects were mild and included increased number of ring-shaped mitochondria.
**, Increased number of ring-shaped mitochondria likely due to rapid sperm depletion (Kubagawa et al., 2006).

Supplemental Experimental Procedures

C. elegans genetics and strains

C. elegans were maintained on NGM plates with NA22 bacteria at 20 °C (Brenner, 1974) except where indicated otherwise. The following strains were used:
DG1743 [*fog-3(q443)/hT2(qIs48)I*] (Miller et al., 2003)
CZ337 [*vab-1(dx31)II*] (George et al., 1998)
CB4108 [*fog-2(q71)V*] (Schedl and Kimble, 1988)
CX3198 [*sax-3(ky123)X*] and CX3171 [*sax-3(ky200)X*] (Zallen et al., 1998)
CB3241 [*clr-1(e1745)II*] (Kokel et al., 1998)
CX5000 [*slt-1(eh15)X*] (Hao et al., 2001)
vpr-1(tm1411)/hT2(qIs48)I (Tsuda et al., 2008)
NL3321 [*sid-1(pk3321)V*] (Winston et al., 2002)
Strain construction and marker scoring were performed essentially as previously described using PCR and phenotypic analyses (Miller et al., 2003; Tsuda et al., 2008). *vpr-1(tm1411)* is a maternal effect sterile mutation and all phenotypes were scored in the F_2 homozygotes derived from heterozygous moms.

RNA-mediated interference

RNAi was performed by the feeding method (Timmons et al., 2001; Timmons and Fire, 1998) starting at the L1 stage or using transgenic methods. RNAi HT115 bacterial feeding strains are from the genome-wide library (Kamath and Ahringer, 2003). All clones were sequenced for confirmation, except for those yielding negative results in the RNAi screens. For tissue-specific RNAi, we generated transgenic lines for expressing antisense and sense RNA in muscle of systemic RNAi deficient *sid-1(pk3321)* mutant worms. SID-1 acts as a channel for importing dsRNA (Winston et al., 2002). For muscle-specifc *sax-3* RNAi, *myo-3p::sax-3::mCherry* (40ng/µl) and *myo-3p::sax-3 antisense* (100ng/µl) plasmids were mixed with the mitochondrial marker *myo-3p::mitoGFP* (60ng/µl) plasmid. For muscle-specific *clr-1* RNAi, *myo-3p::clr-1 antisense* (100ng/µl) was mixed with *myo-3p::mitoGFP* (60ng/µl). Plamids were injected into gonads of adult *sid-1(pk3321)* mutant hermaphrodites. Transgenic progeny were selected based on the GFP expression. Muscle mitochondrial morphology was visualized by mitoGFP.

Plasmid construction

The *vpr-1* and human *vapb* pan-neuronal expression vectors were made by cloning the *vap* ORF into the pBY103 plasmid, which contains the *unc-119* promoter (Maduro and Pilgrim, 1995). The *vpr-1* ORF was amplified by PCR using primers containing PstI and BamHI restriction sites. For muscle specific expression, the *vpr-1* ORF was amplified by PCR using primers containing KpnI and XbaI and cloned into the pPD95.86 vector, which contains the *myo-3* muscle promoter (Okkema et al., 1993). For gut specific expression, ~2.5kB upstream of the *ges-1* initiating methionine (Inoue et al., 2005) was amplified and cloned into the SphI and SalI sites of pPD95.81. The *vpr-1* ORF was inserted in frame into the pPD95.81::*ges-1p* backbone using BamHI and SmaI restriction sites. To determine the *vpr-1* expression pattern, we used PCR to amplify the 2237bp promoter region upstream of *vpr-1* and inserted this genomic region into the pPD95.81 vector upstream of GFP. The translational fusion was made using PCR to amplify the 2237bp promoter region upstream of *vpr-1* and the *vpr-1* genomic locus including introns. For the transcriptional fusion, the 2.3kb of genomic DNA upstream of the *vpr-1* translational start site was amplified by PCR and cloned into the pPD95.81 vector. The *vpr-1* P56S mutant was synthesized by Genescript (Piscataway, NJ) and inserted into the pBY103 plasmid.

Multiple constructs were generated using the MultiSite Gateway Three Fragment kit (Invitrogen). To observe VPR-1 cleavage and secretion, an *unc-119p::mCherry::VPR-1::GFP* plasmid was constructed. *unc-119p*-pDONR P4-P1R plasmid was purchased from Open Biosystems (Huntsville, AL). *mCherry* was amplified from pCFJ90 using PCR and cloned into the pDONR221 vector. *vpr-1* ORF::GFP::*unc-54* 3' UTR was amplified by PCR from *vpr-1* ORF-pPD95.81 and cloned into pDONR P2R-P3 vector. These three plasmids were mixed with LR clonase plus II enzyme mix and pDEST R4-R3 vector II for LR reaction, according to the manufacturer's instructions. This construct contained a G to A mutation at the seventh nucleotide of *vpr-1* causing a conservative glutamic acid to lysine change at the 3rd amino acid. This change lies at the N-terminus outside of the MSP domain and was not anticipated to affect function. To express *sax-3* in muscle, the *sax-3* ORF was amplified using PCR from a plasmid containing 3xFLAG::SAX-3 (kindly provided by J. Culotti) and cloned into pDONR 221 vector. *myo-3p*-pDONR P4-P1R, *sax-3* ORF-pDONR 221, *mCherry::unc-54* 3' UTR-pDONR P2R-P3 and pDEST R4-R3 vector II were reacted with LR clonase plus II enzyme mix. For tissue-specific RNAi of *sax-3* and *clr-1*, antisense constructs were cloned. Inverted *sax-3* ORF was amplified from the 3xFLAG::SAX-3 plasmid using PCR and cloned into pDONR 221 vector. Inverted *clr-1* cDNA was amplified from the CLR-1::V5 plasmid and cloned into pDONR 221 vector. *myo-3p*-pDONR P4-P1R, *unc-54* 3' UTR-pDONR P2R-P3, and pDEST R4-R3 vector II were used for LR reaction. A pJWZ6 plasmid containing the *Drosophila* moesin actin binding domain (kindly provided by Dave Sherwood) was amplified using PCR and inserted into pDONR 221. GFP::*unc-54* 3' UTR was amplified using PCR from the *mitoGFP* plasmid and clonied into pDONR P2R-P3 vector. moesin-pDONR 221, GFP::*unc-54* 3' UTR-pDONR P2R-P3, *myo-3p*-pDONR P4-P1R, and pDEST R4-R3 vector II were used for LR reaction. The following primers were used:

vpr1-10bpcodePstIFP: 5'-CGCCTGCAGCAGCAAAAAAATGTCTGAAAAG-3'
vpr1code-stop BamHIRP: 5'-CGGGGATCCTCTCATTAGAAAAGACGGCCAACAATAAG-3'
vpr-1 KpnISTOPRP: 5'-ACCGGTACCTCATTAGAAAAGACGGCCAACAA -3'
vpr-1 XbaIFP: 5'-GACTCTAGAATGTCTGAAAAGCACAGTCTTC-3'
vpr1codingPstIFP: 5'-CGCCTGCAGATGTCTGAAAAGCACAGTCTTC-3'
vpr-1p2237RP3: 5'-CGGGGATCCTCGAACACGAGTTCACGATTTGG-3'
OP12HindIII2118FP: 5'-GCGAAGCTTACGCGCATTGCCAC-3'
Op12BamHIp2237RP3: 5'-CGGGGATCCTCGAACACGAGTTCACGATTTGG-3'
mcherry 221F: 5'-GGGGACAAGTTTGTACAAAAAAGCAGGCTTAATGGTCTCAAAGGGTGAAGA-3'
mcherry 221R: 5'-GGGGACCACTTTGTACAAGAAAGCTGGGTACTTATACAATTCATCCATGCCA-3'
vpr-1 p4-p1F: 5'-GGGGACAGCTTTCTTGTACAAAGTGGAGATGTCTGAAAAGCACAGTCTT-3'
unc-54 UTR p4-p1R: 5'-GGGGACAACTTTGTATAATAAAGTTGAAACAGTTATGTTTGGTATATTGG-3'
dmoesin 221F: 5'-GGGGACAAGTTTGTACAAAAAAGCAGGCTCCATGGACGAAGTGGAAGACGCCC-3'
dmoesin 221R: 5'-GGGGACCACTTTGTACAAGAAAGCTGGGTACATGTTCTCAAACTGATCGAC-3'
GFP p2-p3F: 5'-GGGGACAGCTTTCTTGTACAAAGTGGAAATGAGTAAAGGAGAAGAACTTTT-3'
sax-3 anti221F: 5'-GGGGACAAGTTTGTACAAAAAAGCAGGCTCAAGTTTGTTCTTGTGTGACGATTCC-3'
sax-3 anti221R: 5'-GGGGACCACTTTGTACAAGAAAGCTGGGTACGAAGCTTCTGCGAAGATGC-3'
clr-1 anti221F: 5'-GGGGACAAGTTTGTACAAAAAAGCAGGCTCACATCAATTCTCCTATATGTGC-3'
clr-1 anti221R: 5'-GGGGACCACTTTGTACAAGAAAGCTGGGTAATGCGAATAAATCGATGGATC-3'

Transgenics

Transgenic lines were generated by microinjection. Plasmids (60ng/µl) were mixed with markers pRF4 [*rol-6*] (60ng/µl) or *myo-3p::mitoGFP* (60ng/µl) (Labrousse et al., 1999) and injected into the gonads of young adult hermaphrodites using a Zeiss Axiovert 200 microscope and Narishige IM-30 microinjector. After 12 hours, injected worms were transferred to new NGM plates and allowed to lay embryos. Transgenic progeny were selected based on the roller

phenotype or GFP expression. Multiple independent transgenic lines were generated and analyzed.

MSP binding assay and receptor identification

Recombinant MSP-6His and human VAP MSP domain-6His were expressed and purified from *E. coli* as previously described (Miller et al., 2001; Miller et al., 2003; Tsuda et al., 2008). The purified proteins were dialyzed using Slide-A-Lazer dialysis cassettes (Pierce, U.S.A) in PBS solution and protein concentrations were determined by the BCA protein assay (Pierce, U.S.A). To visualize MSP binding on oocyte and sheath surfaces, recombinant 6His-MSP was labeled with NHS-Fluorescein (Pierce, U.S.A) at 23°C in the dark for 3 hours, according to the manufacturer's instructions. An excellulose desalting column (Pierce, U.S.A) was used to remove unreacted NHS-Fluorescein. Binding assays were conducted as previously described with minor modification (Miller et al., 2003; Tsuda et al., 2008). Briefly, gonads were dissected in M9 buffer and incubated with 200 nM MSP-FITC or human VAPB MSP-FITC for 20 minutes. Gonads were then washed three times with M9 buffer, lightly fixed in 1% paraformaldehyde for 5 minutes, and mounted on 2% agarose slides. MSP-FITC binding was quantified using AxioVision software (Zeiss, Germany). For normalization, fluorescence intensity in the most proximal oocyte was subtracted from fluorescence intensity in the distal gonad or uterus. Gonads were preincubated with a 20-fold molar excess of unlabelled MSP (or vMSP) to evaluate non-specific binding. For the RNAi screen, 40 potential receptors were selected based on sequence data and published *in situ* hybridization and microarray data (Kohara, 2001; Reinke et al., 2004). We primarily considered the microarray dataset comparing mutant adult hermaphrodites undergoing oogenesis to those undergoing spermatogenesis, given that MSP-FITC receptors are expressed in oocytes, but not sperm. The six receptors identified in the screen all show mRNA expression in the adult germ line by *in situ* hybridization. The tested RNAi clones and results are shown in Table S2.

Paraquat resistance

Resistance to paraquat (Ultra Scientific, U.S.A) was determined as described previously with slight modification (An and Blackwell, 2003; Leiers et al., 2003). Briefly, worms were placed in tubes containing 100 µl of 0, 50, 100, or 150 mM paraquat in M9 buffer and incubated for 24 hours at 20°C. After the incubation, the worms were transferred to watch glasses containing 1ml M9 solution to examine survival. Worms were scored as dead based on failure to respond to gentle touching. Each genotype was analyzed in triplicate and measurements were performed at least three times.

ATP concentration measurement

ATP concentration was measured as described previously, with slight modification (Braeckman et al., 2002; Dillin et al., 2002). Briefly, 150 worms were individually picked and placed into tubes containing M9 buffer, washed four times, and incubated at 20°C for 40 minutes to remove intestinal bacteria. These worms were then washed four times with TE solution (100 mm Tris–Cl, pH 7.6, 4 mm EDTA) and placed into microfuge tubes containing 300 µl TE solution. Worm extracts were prepared by a series of cycles including freezing in liquid nitrogen, thawing, and sonicating. After this process, the extracts were boiled for 10 minutes to release ATP and block ATPase activity. Carcasses and insoluble material were pelleted in a microcentrifuge at 20,000 g for 10 minutes. The soluble extracts were diluted in a 1:10 ratio using TE solution. ATP concentration in 60 µl of diluted extracts was measured using the ENLITEN ATP Assay System (Promega, U.S.A) according to the manufacturer's instructions. A

luminometer (Berthold, Germany) was used for quantification. Protein concentration in worm extracts was determined using the BCA protein assay (Pierce, U.S.A). ATP measurements were repeated at least three times for each strain, although only one experiment is shown. All measurements produced consistent results.

Mitotracker CMXRos and Rhodamine 6g staining

To evaluate mitochondrial membrane potential, MitoTracker CMXRos (Molecular Probes, U.S.A) was incubated with live hermaphrodites (Kubagawa et al., 2006). MitoTracker CMXRos is a lipophilic cationic fluorescent dye whose accumulation in mitochondria is dependent on inner membrane potential (Gilmore and Wilson, 1999). Briefly, 1 mM MitoTracker CMXRos stock was prepared in DMSO. 10 µl MitoTracker CMXRos stock solution was mixed with 40 µl NA22 bacteria and 50 µl M9 solution. This solution was then dropped onto NGM plates and allowed to dry. L4 stage worms were transferred to these NGM plates and incubated in the dark at 20°C for 12 hours. After the incubation, worms were transferred to new NGM plates and incubated in the dark for 20 minutes to reduce background. Worms were mounted for microscopy on 2% dried agarose pads. Wild-type and *vpr-1(tm1411)* mutant hermaphrodites were cultured on the same plates. For Rhodamine 6g staining, the dye was added to seeded plates at a final concentration of 2.5 µg/ml. Worms were incubated on the plates in the dark for at least two days.

Oxygen consumption assays

Oxygen consumption rates were measured as previously described using the oxygraph system (Hansatech, UK) with slight modifications (Braeckman et al., 2002; Yang et al., 2010). Worms were synchronized and grown to the L4 stage at 20°C. These L4 worms were transferred to new NGM plates and incubated for an additional 24 hours at 20°C. To measure oxygen consumption, 1000 worms for each strain were individually picked and placed into glass culture tubes containing 1ml M9 buffer at 20°C. Worms were washed three times, incubated for 40 minutes at 20°C to remove intestinal bacteria and washed five times with M9 buffer. 1000 worms in 1ml M9 were placed into the chamber equipped with a S1 Clark type polarographic oxygen electrode disc. The chamber was maintained at 20°C using a constant-temperature circulating water bath and the oxygen concentration was measured for at least 10 minutes. Worms were carefully collected from the chamber for protein quantification. Rates were normalized to either total protein content or the number of worms. We performed at least three independent measurements per strain.

Supplemental References

An, J.H. and Blackwell, T.K. (2003). SKN-1 links C. elegans mesendodermal specification to a conserved oxidative stress response. Genes Dev *17*, 1882-1893.

Bateman, J., Shu, H., and Van Vactor, D. (2000). The guanine nucleotide exchange factor trio mediates axonal development in the Drosophila embryo. Neuron *26*, 93-106.

Braeckman, B.P., Houthoofd, K., De Vreese, A., and Vanfleteren, J.R. (2002). Assaying metabolic activity in ageing Caenorhabditis elegans. Mech Ageing Dev *123*, 105-119.

Brenner, S. (1974). The genetics of Caenorhabditis elegans. Genetics *77*, 71-94.

Debant, A., Serra-Pages, C., Seipel, K., O'Brien, S., Tang, M., Park, S.H., and Streuli, M. (1996). The multidomain protein Trio binds the LAR transmembrane tyrosine phosphatase, contains a protein kinase domain, and has separate rac-specific and rho-specific guanine nucleotide exchange factor domains. Proc Natl Acad Sci U S A *93*, 5466-5471.

Dillin, A., Hsu, A.L., Arantes-Oliveira, N., Lehrer-Graiwer, J., Hsin, H., Fraser, A.G., Kamath, R.S., Ahringer, J., and Kenyon, C. (2002). Rates of behavior and aging specified by mitochondrial function during development. Science *298*, 2398-2401.

George, S.E., Simokat, K., Hardin, J., and Chisholm, A.D. (1998). The VAB-1 Eph receptor tyrosine kinase functions in neural and epithelial morphogenesis in C. elegans. Cell *92*, 633-643.

Gilmore, K., and Wilson, M. (1999). The use of chloromethyl-X-rosamine (Mitotracker red) to measure loss of mitochondrial membrane potential in apoptotic cells is incompatible with cell fixation. Cytometry *36*, 355-358.

Govindan, J.A., Nadarajan, S., Kim, S., Starich, T.A., and Greenstein, D. (2009). Somatic cAMP signaling regulates MSP-dependent oocyte growth and meiotic maturation in C. elegans. Development *136*, 2211-2221.

Han, S.M., Cottee, P.A., and Miller, M.A. (2010). Sperm and oocyte communication mechanisms controlling C. elegans fertility. Dev Dyn *239*, 1265-1281.

Hao, J.C., Yu, T.W., Fujisawa, K., Culotti, J.G., Gengyo-Ando, K., Mitani, S., Moulder, G., Barstead, R., Tessier-Lavigne, M., and Bargmann, C.I. (2001). C. elegans slit acts in midline, dorsal-ventral, and anterior-posterior guidance via the SAX-3/Robo receptor. Neuron *32*, 25-38.

Kamath, R.S., and Ahringer, J. (2003). Genome-wide RNAi screening in Caenorhabditis elegans. Methods *30*, 313-321.

Kohara, Y. (2001). Systematic analysis of gene expression of the C. elegans genome. Tanpakushitsu Kakusan Koso *46*, 2425-2431.

Kokel, M., Borland, C.Z., DeLong, L., Horvitz, H.R., and Stern, M.J. (1998). clr-1 encodes a receptor tyrosine phosphatase that negatively regulates an FGF receptor signaling pathway in Caenorhabditis elegans. Genes Dev *12*, 1425-1437.

Kubagawa, H.M., Watts, J.L., Corrigan, C., Edmonds, J.W., Sztul, E., Browse, J., and Miller, M.A. (2006). Oocyte signals derived from polyunsaturated fatty acids control sperm recruitment in vivo. Nat Cell Biol *8*, 1143-1148.

Labrousse, A.M., Zappaterra, M.D., Rube, D.A., and van der Bliek, A.M. (1999). C. elegans dynamin-related protein DRP-1 controls severing of the mitochondrial outer membrane. Mol Cell *4*, 815-826.

Leiers, B., Kampkotter, A., Grevelding, C.G., Link, C.D., Johnson, T.E., and Henkle-Duhrsen, K. (2003). A stress-responsive glutathione S-transferase confers resistance to oxidative stress in Caenorhabditis elegans. Free Radic Biol Med *34*, 1405-1415.

Maduro, M., and Pilgrim, D. (1995). Identification and cloning of unc-119, a gene expressed in the Caenorhabditis elegans nervous system. Genetics *141*, 977-988.

Miller, M.A., Nguyen, V.Q., Lee, M.H., Kosinski, M., Schedl, T., Caprioli, R.M., and Greenstein, D. (2001). A sperm cytoskeletal protein that signals oocyte meiotic maturation and ovulation. Science *291*, 2144-2147.
Miller, M.A., Ruest, P.J., Kosinski, M., Hanks, S.K., and Greenstein, D. (2003). An Eph receptor sperm-sensing control mechanism for oocyte meiotic maturation in Caenorhabditis elegans. Genes Dev *17*, 187-200.
Okkema, P.G., Harrison, S.W., Plunger, V., Aryana, A., and Fire, A. (1993). Sequence requirements for myosin gene expression and regulation in Caenorhabditis elegans. Genetics *135*, 385-404.
Reinke, V., Gil, I.S., Ward, S., and Kazmer, K. (2004). Genome-wide germline-enriched and sex-biased expression profiles in Caenorhabditis elegans. Development *131*, 311-323.
Schedl, T., and Kimble, J. (1988). fog-2, a germ-line-specific sex determination gene required for hermaphrodite spermatogenesis in Caenorhabditis elegans. Genetics *119*, 43-61.
Steven, R., Kubiseski, T.J., Zheng, H., Kulkarni, S., Mancillas, J., Ruiz Morales, A., Hogue, C.W., Pawson, T., and Culotti, J. (1998). UNC-73 activates the Rac GTPase and is required for cell and growth cone migrations in C. elegans. Cell *92*, 785-795.
Timmons, L., Court, D.L., and Fire, A. (2001). Ingestion of bacterially expressed dsRNAs can produce specific and potent genetic interference in Caenorhabditis elegans. Gene *263*, 103-112.
Timmons, L., and Fire, A. (1998). Specific interference by ingested dsRNA. Nature *395*, 854.
Tsuda, H., Han, S.M., Yang, Y., Tong, C., Lin, Y.Q., Mohan, K., Haueter, C., Zoghbi, A., Harati, Y., Kwan, J.*, et al.* (2008). The amyotrophic lateral sclerosis 8 protein VAPB is cleaved, secreted, and acts as a ligand for Eph receptors. Cell *133*, 963-977.
Watari-Goshima, N., Ogura, K., Wolf, F.W., Goshima, Y., and Garriga, G. (2007). C. elegans VAB-8 and UNC-73 regulate the SAX-3 receptor to direct cell and growth-cone migrations. Nat Neurosci *10*, 169-176.
Winston, W.M., Molodowitch, C., and Hunter, C.P. (2002). Systemic RNAi in C. elegans requires the putative transmembrane protein SID-1. Science *295*, 2456-2459.
Wolke, U., Jezuit, E.A., and Priess, J.R. (2007). Actin-dependent cytoplasmic streaming in C. elegans oogenesis. Development *134*, 2227-2236.
Wong, K., Ren, X.R., Huang, Y.Z., Xie, Y., Liu, G., Saito, H., Tang, H., Wen, L., Brady-Kalnay, S.M., Mei, L.*, et al.* (2001). Signal transduction in neuronal migration: roles of GTPase activating proteins and the small GTPase Cdc42 in the Slit-Robo pathway. Cell *107*, 209-221.
Yang, Y., Han, S.M., and Miller, M.A. (2010). MSP hormonal control of the oocyte MAP kinase cascade and reactive oxygen species signaling. Dev Biol *342*, 96-107.
Zallen, J.A., Yi, B.A., and Bargmann, C.I. (1998). The conserved immunoglobulin superfamily member SAX-3/Robo directs multiple aspects of axon guidance in C. elegans. Cell *92*, 217-227.